Miner Petrol (2011) 101:115–128
DOI 10.1007/s00710-010-0138-2

ORIGINAL PAPER

Pyrite tracks assimilation of crustal sulfur in Pyrenean peridotites

Jean-Pierre Lorand · Olivier Alard

Received: 18 January 2010 / Accepted: 5 October 2010 / Published online: 3 November 2010

Abstract Cobalt-bearing pyrite (0.5–2.0 wt.% Co) is abnormally abundant (up to 35 vol.% of the total volume of the sulfide phase) in some eastern Pyrenean peridotite massifs, compared to pieces of subcontinental mantle studied so far for sulfides. Pyrite occurs as vermicular intergrowths inside pentlandite and/or chalcopyrite or as coarser, blocky grains in the intergranular pores of host peridotites. Those different pyrites are characterized by different platinum-group element systematics (measured by laser ablation microprobe and ICP-MS). Vermicular pyrite intergrown with pentlandite displays Os-, Ir-, Ru- and Rh-enriched chondrite normalized PGE patterns of Monosulfide solid solution (Mss). In contrast, coarse-grained intergranular ("blocky") pyrites, are PGE-poor. Chalcophile trace elements (i.e. Zn, Pb, Ag, Au) that are not usually concentrated in mantle-derived sulfides were commonly detected. By contrast, selenium contents are generally low, yielding thus pyrite with high S/Se ratio ($>10^5$), consistent with a sedimentary sulfur source. Pyrite microtextures and chalcophile trace element contents support a process of assimilation of crustal sulfur from the metamorphosed sedimentary country rocks. These latter generated highly reactive CO_2-S fluids, which were injected into structural discontinuities of the lherzolitic bodies. Sulfur has reacted at T=300–550°C with pre-existing, mantle-derived, metal-rich sulfide assemblages (pentlandite-chalcopyrite). Addition of crustal sulfur did produce Mss which, on cooling, exsolved the Os-rich pyrite in addition to pentlandite. The coarse-grained pyrite types have crystallized directly from S-rich fluids.

Editorial handling: J. Raith

J.-P. Lorand (✉)
Laboratoire de Minéralogie et Cosmochimie (CNRS UMR 7202),
Muséum National d'Histoire Naturelle,
CP 52, 61 Rue Buffon,
75005 Paris, France
e-mail: Jplorand@mnhn.fr

O. Alard
Géosciences Montpellier, CNRS UMR 5243,
Université de Montpellier II,
Cc 60, Place Eugène Bataillon,
34095 Montpelier Cédex, France

Introduction

Pyrite is a late phase in magmatic rocks. It crystallizes upon oxidation of pyrrhotite or assimilation of sulfur from country rocks, which triggers sulfurisation reactions (e.g. Naldrett and Gasparini 1971; Duke and Naldrett 1976; Hall 1986). Pyrite has also been described as deuteric oxidation products after mantle-derived sulfides in peridotite xenoliths and in talc-carbonate alteration of serpentinites (Eckstrand 1975; Klein and Bach 2009). Hydrothermal pyrite is common in extensively serpentinised oceanic peridotites (e.g. External Ligurides; Luguet et al. 2004). By contrast, pyrite is not expected to exsolve from mantle-derived sulfides (pentlandite, chalcopyrite or pyrrhotite), because (a) pentlandite and pyrite are an incompatible mineral pair above ca. 282°C (Craig 1973; Misra and Fleet 1973) and (b) silicate-sulfide assemblages of unaltered mantle-derived rocks buffer the fugacities of oxygen and sulfur close to the FMQ-Po buffer, i.e. below the required level for pyrite formation (Eggler and Lorand 1993). Indeed, detailed investigations of various mantle-derived peridotites worldwide did not reveal the occurrence of significant amounts of pyrite (e.g. Garuti et al. 1984; Lorand 1985, 1991; Kogiso et al. 2008).

Orogenic peridotites from the northeastern part of the French Pyrénées are unique in that, despite very weak

serpentinisation, they are unusually rich in pyrite (accounting for up to 35% by volume of base metal sulfides (BMS), otherwise represented by pentlandite (Pn), chalcopyrite (Cp) or Pyrrhotite (Po); Lorand 1989a, b; Fabriès et al. 1989). Lorand (1989b) ascribed the pyrite a subsolidus origin (i.e. exsolution product of mantle-derived sulfides) because (a) pyrite shows a high Co contents (up to 2 wt.% Co; Co/Ni=2–3) and (b) vermicular pyrite forms "eutectoid" microtextures with pentlandite. Such textures are not known from any other massive peridotites studied so far for BMS. To better constrain the origin and timing of crystallization of the pyrite with respect to the three other BMS, five samples from the most pyrite-rich Pyrenean lherzolitic massifs were investigated in detail by reflected light and scanning electron microscopy. Then, the BMS phases were analysed for chalcophile trace elements (i.e. platinum-group elements, Se, Te, Zn, As, Sb, Bi) using laser-ablation microprobe (LAM) ICP-MS analysis. It will be shown that sulfide microtextures and geochemistry, particularly S/Se ratios and PGE partitioning behaviour are at variance with Lorand's (1989b) conclusion and suggest assimilation of external sulfur during the emplacement of peridotite bodies into the upper crust.

Geological setting

Seven clusters of subcontinental mantle slices, varying in size from a few meters to two or three square kilometres occur along the North Pyrenean Fault (NPF), a major transcurrent lithospheric fault, which separates the Iberian plate from the European plate (Fig. 1). Peridotites (lherzolites) are scattered within the North Pyrenean Zone (NPZ) of Mesozoic sediments paralleling the NPF (Monchoux 1970; Fabriès et al. 1991, 1998). These subcontinental mantle pieces were exhumed during the mid-Cretaceous, extreme continental thinning along the NPZ during the opening of Albian–Cenomanian pull-apart sedimentary basins resulting from the counter-clockwise rotation of Spain relative to Western Europe (Vielzeuf and Kornprobst 1984; Lagabrielle and Bodinier 2008).

Pre-Albian, sedimentary rocks in the pull apart basins consist of metasediments a) Triassic salt deposits, b) Liassic sediments (meta-evaporites, calcareous pelitic sandstones, argillites and shales representing lagoonal deposits) Jurassic to Eocretaceous dolomitic limestones (Ravier and Thiébaut 1982; Montigny et al. 1986; Lagabrielle and Bodinier 2008). Along the North-Pyrenean Fault (NPF) in the North Pyrenean metamorphic zone (NPMZ) that bounds the Pyrenean Axial Zone to the north, those metasediments were affected by a HT-LP mid-Cretaceous thermal metamorphic event (known as «Pyrenean» metamorphism) which lasted almost 25 Ma between 110 and 85 Ma (Montigny et al. 1986; Golberg and Maluski 1988; Dauteuil and Ricou 1989). Shales and calcareous pelitic sandstones were metamorphosed to micaschists/ hornfels and Jurassic-Eocretaceous dolomitic limestones to marbles, respectively. The most typical high-grade metamorphic assemblages include scapolite, phlogopite/biotite, diopside, K-feldspar and locally dolomite and tourmaline. Pyrite is a most widespread accessory mineral in all metasediments of the NPMZ. Metamorphic peak conditions documented by Golberg and Leyreloup 1990) involve temperatures close to 550–650°C for a maximum pressure of 0.3–0.4 GPa. Metamorphic reactions involving salt-derived products and carbonates released hot, alkaline-rich H_2O–CO_2–Cl fluids which transported Cl, Na, Ba, B, Mg, K, P and S in the upper part of the sedimentary sequence. As shown by Golberg and Leyreloup (1990), fracturing played an essential role in heat and fluid transfer, which explains the heterogeneity of the distribution of isograds as well as for the rapid lateral changes of temperature gradients at a km scale (see also Dauteuil and Ricou 1989).

The Py-bearing peridotites are all located in Eastern Pyrenean (EP) peridotites which occur in the Ariège department, in the north-eastern Pyrenees (Fig. 1). There, NPMZ metasediments form narrow discontinuous zones of Jurassic-Early Cretaceous limestones, marbles, dolomites, rare metapelites and voluminous flysch and polymictic breccias deposits (Prades, Tarascon and Aulus basins; Monchoux 1970; Lagabrielle and Bodinier 2008). Although minute pyrite crystals may be found in each of the twenty three peridotite occurrences known in Ariège, pyrite is basically a major BMS only in the small bodies (less than 300 m in length) of Fontête Rouge, Porteteny, Sem, Pic Couder (Lherz-Vicdessos group), and Caussou, Bestiac, Pic de Calmont, (Prades-Bestiac area; Fig. 1b). These peridotite occurrences are very weakly serpentinized (<<1–8% Lorand 1989a, b; Fabriès et al. 1991). Eastern Pyrenean mantle tectonic lenses are either in fault contact with large volumes of strongly deformed Triassic metasediments (including meta-evaporites) or with Jurassic and Lower Cretaceous sediments belonging to the cover of the NPZ. All contacts of Eastern Pyrenea lherzolites are strongly brecciated. Very reactive siliceous dolomitic limestones have undergone heat-driven decarbonation reactions during Pyrenean metamorphism, causing sudden release of CO_2 which hydraulically fractured both the lherzolitic bodies and their metasedimentary country-rocks (Dauteuil et al. 1987; Dauteuil and Ricou 1989). Inside the peridotite bodies, abundant fracture planes cut across mantle-derived microstructural features. At Fontête Rouge and Caussou, mantle-derived Cr-diopside (Cpx) is commonly altered in poikilitic crystals containing Na-plagioclase, amphibole, scapolite, carbonate micro-inclusions (Conquéré 1978). Exchange reactions between metamorphic limestones and the Caussou

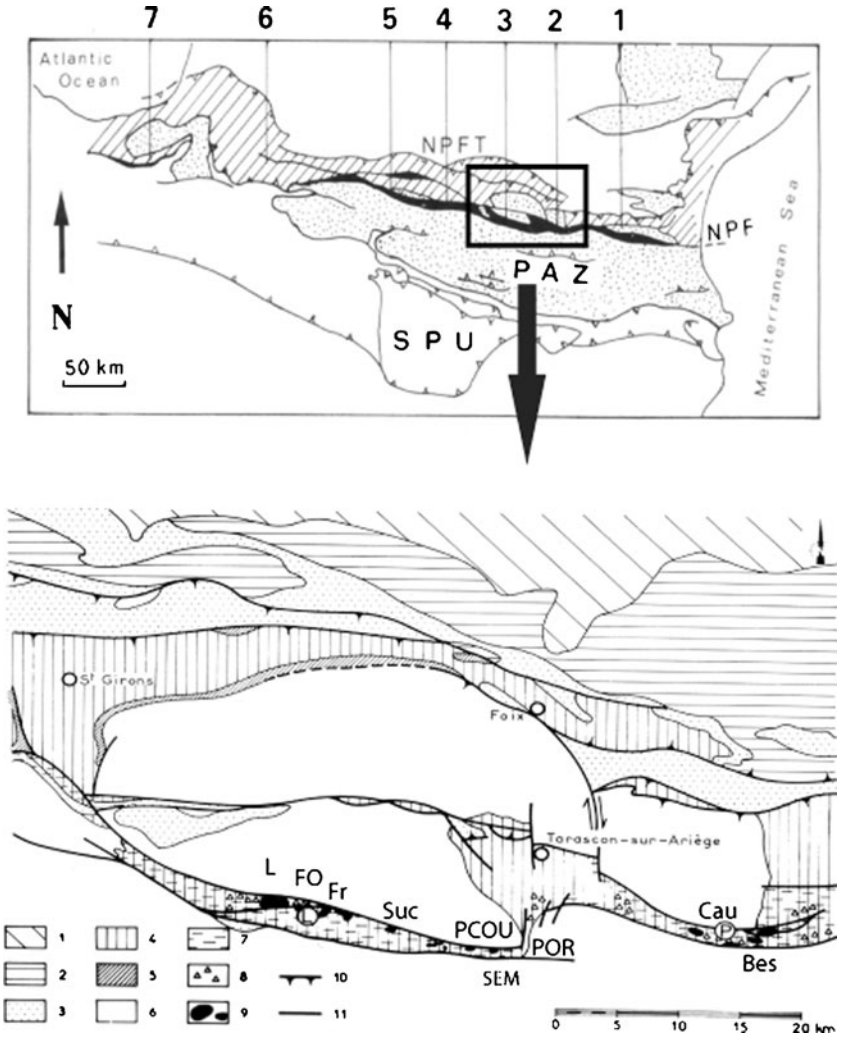

Fig. 1 Structural sketch map showing the location of the different groups of mantle peridotite bodies throughout the Pyrenees (after Fabriès et al 1991). Groups 1 to 3 correspond to Eastern Pyrenean peridotite bodies, Groups 4 to 7 to Western Pyrenean peridotite bodies, respectively (Fabriès et al. 1998). *1*, Salvezines; *2*, Prades-Bestiac group, *3*, Vicdessos-Lherz group; *4*, Arguenos-Tuc d'Esse group; *5*, Avezac-Moncaut group; *6*, Turon de Técouère-Urdach group; *7*, Ciga Dotted areas indicates Hercynian and older rocks (North Pyrenean Massifs and the Paleozoic axial zone-PAZ). *Oblique* ruling indicates Mesozoic sediments of the North Pyrenean Zone and equivalents. The area shown in *black* in the North Pyrenean Metamorphic Zone (NPMZ). *SPU* South Pyrenean Units; *NPF* North Pyrenean Fault; *NPFT* North Pyrenean Frontal Thrust. *Bottom*: details of the eastern Pyrenean peridotite bodies. *L* Lherz; *Fo* Fontête Rouge; *Fr* Freychinède; *Suc* Suc en Sentenac; *PCOU* Pic Couder; *POR* Porteteny; *SEM* Sem (Vicdessos-Lherz); *Cau* Caussou; *Bes* Bestiac; *PC* Pic de Calmont (Prades-Bestiac cluster)*1*: post-tertiary terrains; Eocene; *3* Middle to Upper Cretaceous; *4* Pre-Cenomanian mesozoïc; *5*: Trias; *6*: Hercynian granitoïds; *7*: high-temperature, low-presure metamorphism; *8*: breccias; *9* peridotite bodies; *10–11*: faults and thrust zones. After Conquéré and Fabriès (1984)

peridotites were also suggested from radiogenic isotope systematics (Sr, Nd) and gold enrichment (Downes et al 1991; Lorand et al. 1999). Low-density CO_2 (0.7–0.8 g.cm^3)–rich fluids indicate trapping pressures <0.5 GPa at Caussou (Fabriès et al. 1989).

Analytical methods

The five samples analysed were selected from a list of 30 samples investigated in previous studies of base metal sulfides in Pyrenean orogenic peridotites. The selected samples were studied in polished thin sections with reflected light microscopy and Scanning Electron Microscopy (SEM; Supra^{TM} 55VP Zeiss FEG-SEM; Pierre and Marie Curie University, Paris VI). Platinum-group element contents in base metal sulfides were determined along with a few other chalcophile trace elements (Ag, Te, Bi, Pb, Se, Zn) by laser-ablation inductively coupled plasma mass spectrometry (LA-ICP-MS). The laser employed was a GEOLAS excimer UV delivering a 193 nm beam, coupled with an Element II magnetic sector high-resolution spec-

trometer (Geoscience Montpellier; University of Montpellier II). Ablation was carried out using a helium carrier gas (≈0.6 l/min), and ablated products were transferred to the ICP-MS in a pure Ar atmosphere (0.85 l/min). Analytical conditions included a 51 μm beam diameter, a 5 Hz laser frequency and a beam energy of ca 15 J•cm^{-2}. Sulfur contents determined by electron microprobe analysis were used as internal standard. Raw data were processed on-line using the GLITTER software package (Van Achterbergh et al. 2001). Selenium was measured on ^{82}Se to avoid strong interferences with argon. The PGEs were measured in the peak jumping mode on ^{99}Ru, ^{101}Ru, ^{103}Rh, ^{105}Pd, ^{106}Pd and ^{108}Pd, ^{190}Os, ^{192}Os, ^{193}Ir, ^{195}Pt, ^{196}Pt. ^{63}Cu^{40}Ar interference on ^{103}Rh (monoisotopic) was corrected by ablating a PGE-free synthetic Cu metal (PROLABO^{TM}) several times during the run and determining the production rate of ^{63}Cu^{40}Ar (0.0012±0.0006 ^{63}Cu^{40}Ar Cps / ^{63}Cu Cps). The accuracy of the correction was checked by correcting ^{105}Pd for ^{65}Cu^{40}Ar interference and comparing it to ^{108}Pd, which is free of major interference. PGE-A, a PGE-doped NiS sulfide bead was used as an external standard. Information on accuracy and precision were reported by Lorand et al. (2010). Typical detection limits, for the conditions described above, are lower than 40 ppb for PGEs and ca 100–500 ppb for the other chalcophile trace elements included in the analytical pack.

Mineralogy of pyrite-rich sulfide assemblages

Pyrenean lherzolites contain 0.05 to 0.1 wt.% of accessory BMS (Lorand 1989a, 1991) The BMS occur as 0.2 to 0.3 mm wide grains preferentially located within grain boundaries of silicates, mainly at triple junctions of pyroxenes and olivine crystals or attached to Al-spinel crystals. The majority of the intergranular BMS grains display convex-inward curved margins meeting at low dihedral angles (Fig. 2). Sulfides may protrude deeply inside silicate grain boundaries. As BMS inclusions in silicates, Lorand (1989b) distinguished a) isolated inclusions, rounded to ellipsoidal droplets (50×100 μm on average), interpreted as intergranular BMS blebs incorporated into olivine and pyroxene during secondary grain growth in the lithospheric mantle (R1 stage of Conquéré and Fabriès 1984 and Fabriès et al. 1991); b) trails of negative-crystal shaped inclusions associated with CO_2-rich fluid-inclusion arrays (Fabriès et al. 1989). Lorand (1989b) and Lorand et al. (2008, 2010) have extensively documented the sulfide mineral assemblages of Eastern Pyrenean lherzolite massifs. They identified pentlandite (Pn), chalcopyrite (Cp), pyrrhotite (Po), pyrite (Py) and minor secondary sulfides. Except in the pyrite-rich bodies, pentlandite and chalcopyrite (the Ni and Cu-sulfides) totalize more than 95% by volume of the BMS

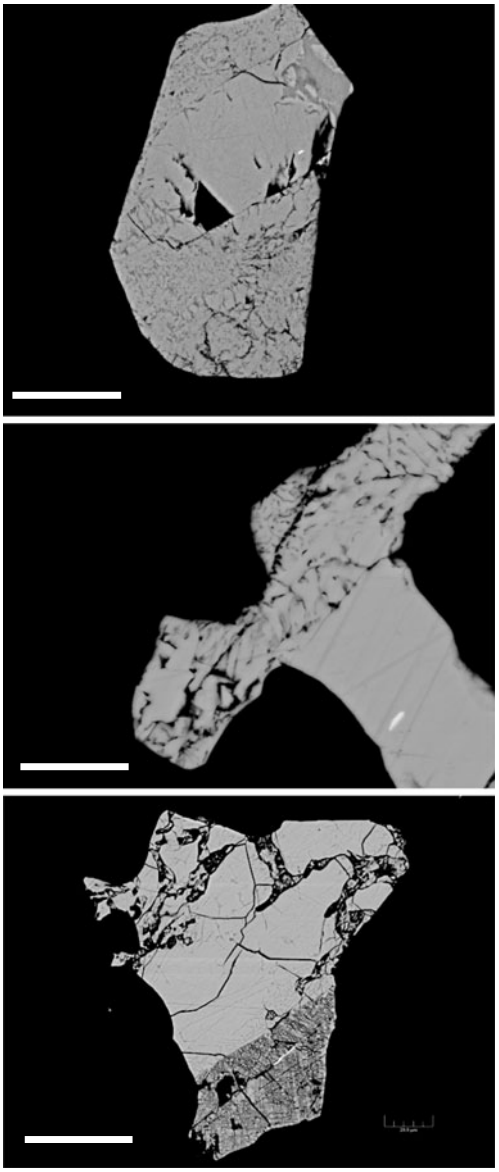

Fig. 2 SEM pictures of pyrite-free pentlandite in Pyrenean peridotites. Note vermicular networks inside each grain. Although shaped as vermicular pyrite, no pyrite was identified in such networks which contain only granulated pentlandite in addition to minute pyrrhotite grains. Scale bar=50 μm

grains. This is especially true for the largest, km-sized massifs (e.g. Lherz, Freychinède, Prades). Blocky pentlandite is by far predominant. It displays curious networks of vermicular holes reminiscent of the vermicular pyrite blebs from eutectoid pentlandite-pyrite microtextures (see below). SEM analyses did not reveal any specific chemical features in those vermicular blebs (Fig. 2). The second most abundant BMS is chalcopyrite, which is mainly associated with pentlandite in two-phase grains. The two sulfides are separated by sharp contacts. Except in the immediate vicinity of pyroxenitic layers, pyrrhotite is usually not present but may occasionally form discrete granules at the

margin of the pentlandite grains (Fig. 3a). Another occurrence of secondary polycrystalline pyrrhotite may fill cavities inside the pentlandite which enclose tens of micrometer-sized pyrite blebs (see Fig. 2 in Lorand 1989b).

Pyrite occur in high proportions (5–35 wt.%) in all the samples investigated so far in the seven pyrite-rich lherzolitic bodies, except where supergene weathering has oxidized the pyrite into Fe oxy-hydroxides (e.g. Porteteny). Fabriès et al. (1989) reported modal abundances of pyrite ranging between 16 and 31 wt.% (for 100 wt.% BMS) in six Caussou lherzolites. The abundance of pyrite in Caussou peridotites does not correlate with any petrogenetic indicator (Mg/Mg + Fe ratio of mafic silicates or Cr/Cr + Al ratio of Al–Cr spinels; REE abundances; modal contents of disseminated amphibole). Secondary inclusions trails cross-cutting silicates are pyrite-rich; almost every inclusion contains 5 to 25 vol.% of pyrite. BMS inclusions are interspersed with CO_2-inclusions. Modal estimates performed on 70 inclusions from a single trail yield Pn56Po5-Py25Cp14. Pyrite occurs mostly as vermicular intergrowths

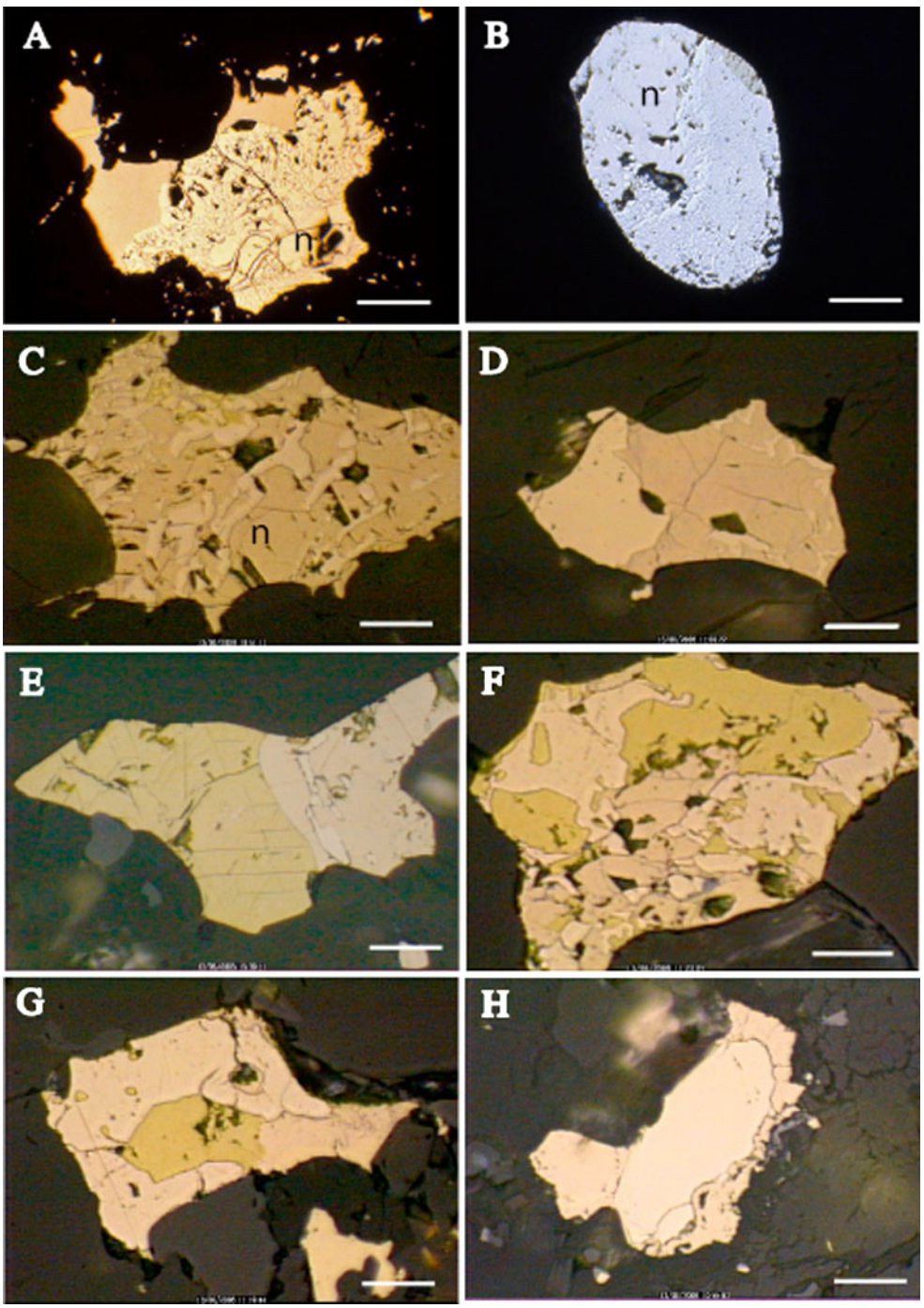

Fig. 3 Plane-polarised reflected light microphotographs of pyrite. Scale bar=50 μm except B (20 μm). **a** "eutectoid" microtextures of pyrite inside blocky pentlandite; *n*=pyrite-free pentlandite nucleus. **b** Pyrite-pentlandite intergrowths in olivine-hosted pseudoprimary sulfide inclusion; *n*=Pyrite-free pentlandite nucleus. **c** Pyrite-rich anhedral pentlandite blebs displaying the denticulated shapes and convex-inward grain boundaries of metal-rich sulfide melt. **d** Coarse-grained pyrite replacing intergranular pentlandite; note that the original shape of pentlandite was preserved. **e** Two-phase chalcopyrite-pentlandite bleb showing pyrite inside the pentlandite. **f** Crystallization of skeletal pyrite across a contact between pentlandite and chalcopyrite. **g** « blocky » pyrite replacing a chalcopyrite-pentlandite two-phase grain; note the spherical inclusions of chalcopyrite and pentlandite inside pyrite which has preserved the shape of original pentlandite and chalcopyrite. **h** Massive (« blocky ») pyrite rimmed with polycrystalline pentlandite

inside pentlandite and/or chalcopyrite or as coarser, blocky grains in the intergranular pores of host peridotites (Fig. 3). Such symplectitic, eutectoid microtextures between pentlandite and pyrite are a unique feature of Eastern Pyrenean orogenic lherzolites. They are also present in the spherical sulfide inclusions that were trapped in recrystallized olivine (Fig. 3b). Such pyrite-bearing inclusions are more abundant in Bestiac peridotites than in any other Eastern Pyrenean peridotite bodies (Lorand 1989b). Defocused beam EMP analyses on symplectitic Py-Pn intergrowths plot within the stability domain of Monosulfide Solid Solution (Mss) in the Fe–Ni–S ternary (Fig. 4).

The five samples studied here (PCOU1, POR1, 70-222, 70-118 and 71-335) are mildly fertile coarse-granular lherzolites ($2.83 < Al_2O_3 < 3.00$ wt.%; Table 1). Modal estimates (recomputed to 100% BMS) indicate 15 to 35 wt. % pyrite (Table 1). Pyrite coexists with Ni-rich Pn ($0.9 < Ni/Fe < 1.2$) and pyrrhotite with composition close to Fe_7S_8 monoclinic-type end member (Fig. 4). By contrast, sample 71-335 is the only Freychinède lherzolite (over five samples examined in reflected light microscopy) to be so rich in pyrite. The main microtextures of pyrite observed in the five samples are illustrated in Fig. 3c–h. Pentlandite-pyrite vermicular intergrowths generally preserve a pyrite-free pentlandite nucleus, also observed in rounded BMS inclusion in olivine (Fig. 3b). In spite of their overall enrichment in pyrite, the five samples may also display pyrite-free pentlandite ± chalcopyrite grains (19 out of 35 grains in PCOU1; two out of 12 in POR1; six out of 45 in 70-222) within a single thin section. In addition to the symplectitic pentlandite-pyrite intergrowth described above, pyrite may either nucleate inside pentlandite as a few tens of μm blebs and/or develop coarse-grained morphology partially replacing the pentlandite at one edge (Fig. 3d, e). Chalcopyrite is either pyrite-free (Fig. 3c, g) or encloses denticulated pyrite blebs which also invade the coexisting pentlandite (Fig. 3f). Pyrite may also replace pentlandite and chalcopyrite, starting from the BMS grain boundaries; this microtexture produces poikiloblastic pyrite enclosing pentlandite and chalcopyrite droplets (Fig. 3g). In each of the microtextures described above, the shape of pre-existing magmatic sulfide grains was preserved, especially the sulfide re-entrants cones inside the grain boundaries of surrounding silicates. Sample 71-335 shows only coarse-granular ("blocky) pyrite grains, always intergranular and occasionally rimmed with polycrystalline pentlandite (Fig. 3h).

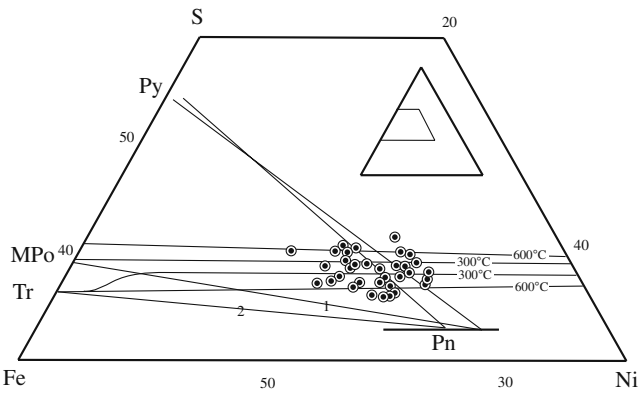

Fig. 4 Composition of intergrowths between pentlandite and pyrite (*dotted circles*; Lorand 1989b). Compositional limits of monosulfide solid solution (MSS) at 300°C and 600°C after Naldrett et al. 1967. Pre-existing metal-rich sulfides (pentlandite) were converted into Mss that exsolved pyrite and/or pentlandite on cooling below 300°C. *Tie*-lines 1 and 2 correspond to the main interstitial sulfide assemblages of the Fe-NiS system identified in Pyrenean peridotites (*1*: pentlandite (Pn)—pyrite (Py)—monoclinic-type pyrrhotite (Po); *2*: pyrite (Py)—pentlandite (Pn)—troilite type pyrrhotite (Tr)

Table 1 Key petrographic data for the pyrite-rich samples

	S ppm	Al_2O_3 wt.%	CaO wt.%	L.O.I. wt.%	Pyrite vol%
Freychinède					
71-335	310	2.72	2.28	1.07	30
Suc Sentenac					
70-222	222	3.4	2.75	0.14	29
Porteteny					
POR-2	271	3.24	3.13	0.04	35
Pic Couder					
PCOU-1	210	2.83	2.88	0.45	11
Caussou					
70-118	320	3	3.22	0.60	25

Data compiled from Fabriès et al. (1989), Lorand (1989a) and Lorand et al. (1999)

LOI loss on ignition

Trace element contents

Due to the scale and microstructural complexity of the sulfide intergrowths, determining the trace element patterns of pure sulfides with a 51 μm laser beam was challenging. Thus, most of the LA-ICPMS analyses represent mix products and those reported in Table 2 must be regarded as "best off" analyses.

Platinum-group elements

Despite the technique limitation mentioned above, the various pyrite types identified in Pyrenean peridotites show specific PGE systematics. The pyrite blebs intergrown with pentlandite (PCOU1 and 70-222) are characterized by high (>1,200 ppm) contents of the iridium-group PGEs (IPGE: Os, Ir, Ru), whereas the platinum-group PGEs (PPGE: Pt,

Pd and Au) are strongly depleted (i.e., Pt = <0.007–0.33 ppm; Pd <0.01 ppm; Au <0.001 ppm; Pt/Ir_N and Pd/Ir_N $<10^{-3}$). Their C1-chondrite normalized PGE patterns ressemble those of residual Monosulfide solid solution identified in basalt-borne peridotite xenoliths (Fig. 5; Alard et al. 2000; Lorand and Alard 2001). A lack of Ru spikes in time-resolved LA-ICP-MS spectra indicates that IPGE + Rh do reside inside the pyrite, and are not sited in laurite ((Ru, Os)S_2) micronuggetts similar to those described in Lherz peridotites (Lorand et al. 2010). The same is also true for As (up to 13 ppm in PCOU1 A#7), which correlates positively with Ru. In 70-222 (and 70-118 A#13), the analyses were contaminated by coexisting pentlandite at the end of the ablation run (pyrite/pentlandite ratio within the spot area ranging between 40/60 to 60/40%). Hence, the corresponding analyses display lower IPGE abundances and higher Pd and Au contents than "pure" pyrite as reported in e.g. PCOU1 A#7. The slight Pt negative anomaly also probably resulted from contamination by coexisting pentlandite which is characteristically highly Pt-depleted in Pyrenean lherzolites (Lorand et al. 2008, 2010). Another source of Pt variation is the occurrence of Pt-Te-Bi micronuggetts, detected by coupled concentration spikes in time-resolved LA-ICP-MS spectra. Coarse-granular pyrite from sample 71-335 is PGE-poor, and the three grains are rather homogeneous regarding the PGE + Au concentrations. These grains display roughly flat C1-normalized PGE patterns, with equal proportions of IPGEs and PPGEs at 5–10×C1 (Fig. 5).

Pentlandite concentrates Pd (from 9.0 ppm in PCOU1 to 22.45 ppm for 70-118 and 28.2-42.6 ppm in 70-222) which generates a positive anomaly in chondrite-normalized PGE patterns despite probable contamination of the analyses by pyrite, are particularly relevant for 70-222 Pn-Py intergrowths (Fig. 5b). The IPGE concentrations of pentlandite depend upon the compositions (and thus microstructural features of coexisting pyrite). Pentlandites from samples PCOU1 and 70-118 are IPGE-depleted (1.4–6.0 ppm Os, 1.1–0.8 ppm Ir; 2.9–0.8 ppm Ru) whereas 70-222 pentlandite is IPGE-rich (19–24.3 ppm Os, 4.85–20.9 ppm Ir, 14.9–22.2 ppm Os). Negative Pt anomalies, the benchmark of pentlandite patterns in orogenic peridotites are very weak where time-resolved LA-ICPMS spectra showed evidence of Pt-Te-Bi micronuggets (70-118 and 70-222; Fig. 5b). Conversely, PCOU1 pyrites, which are free from such nuggets, show deeper negative Pt anomaly ($Pt/Ir_N \leq 0.1$).

Pure chalcopyrite is Au- and PGE-poor (0.002–0.07 ppm; <0.001×CI chondrite, Pd=0.36 ppm; 0.07×CI chondrite). High IPGE and Au concentrations reflect contamination by pyrite (PCOU1) whereas pentlandite contamination (70-222) can be traced by increasing concentrations of PPGEs.

All 70-222 BMS (pentlandite, pyrite, chalcopyrite) are Au-rich (1.19–5.03 ppm) as are 71-335 pyrites (1.65–2.35 ppm Au) whereas PCOU1 and 70-118 BMS are all uniformly depleted in Au (<0.06 ppm). This contrasted distribution likely results from the occurrence of discrete Au microminerals in 70-222 and 71-335 pyrites, as suggested by Au, Ag, Te, Bi and Pb concentration spikes in their time-resolved LAM-ICPMS spectra.

b) chalcogenides (Se, Te, Bi) and chalcophile elements (Ag, Zn, Pb)

The analysed pyrite shows highly fractionated S/Se ratios (2.10^4–3.10^5; Table 2) relative to primary mantle BMS ($S/Se \approx 3.0 \pm 0.5 \bullet 10^3$; Guo et al. 1999; Lorand and Alard 2001; Lorand et al. 2003; Hattori et al. 2002). Selenium and nickel are broadly correlated (Fig. 6). Thus the main Se contributor in the pyrite-rich samples is pentlandite, which is two times richer (up to 260 ppm Se, Table 2) than the pentlandite in pyrite-poor orogenic lherzolites (Lorand et al. 2008, 2010; Luguet et al. 2004) and basalt-borne xenoliths (Lorand and Alard 2001; Hattori et al. 2002). The fine-grained Pn-Py intergrowths exibit intermediate Se contents (100–139 ppm Se in 70-222). Chalcopyrite may also be a Se concentrator as demonstrated by PCOU1 Cp (165 ppm Se; PCOU1 A#12).

Pentlandite is the main concentrator for Zn (58–128 ppm). The concentrations of Te, Bi, Ag, Pb in vermicular pyrite are below detection limits (0.5–0.05 ppm). All four elements are noised by their heterogeneous distribution at the scale of one micrometer, although their concentrations tend to increase where a contribution from pentlandite is obvious (e.g. 70-118 and 70-222). Silver, known to be hosted in chalcopyrite (Barnes et al. 2006) displays highly variable concentrations in these sulfides (0.37–1,067 ppm; 70-222).

Discussion

Lorand (1989b) interpreted the pyrite in Eastern Pyrenean lherzolites as a subsolidus phase exsolved from mantle-derived BMS because (a) pyrite preferentially occurs in peridotites displaying very low serpentinisation degree and (b) bulk-compositions of symplectitic pyrite-pentlandite intergrowths are very akin to the monosulfide solid solution compositions preserved in ultramafic xenoliths of the sub-continental lithospheric mantle ($0.3 < Ni/Fe_{at} < 0.5$; Lorand and Conquéré 1983; Guo et al. 1999; Alard et al. 2000 and references therein). In-situ PGE data lend further support to derivation of vermicular pyrite from a monosulfide solid solution (Mss). However, several features are at variance with Lorand's (1989b) interpretation. These are (a) pyrite-free pentlandite nucleii inside pyrite-pentlandite eutectoid microstructures (b) inclusions of chalcopyrite and pentland-

Table 2 Representative in-situ analyses of pyrite (Py). Pentlandite (Pn) chalcopyrite (Cp) and pyrrohotite (Po) in pyrite-rich lherzolites

Sample	PCOU1						70-118				
Sulf-grain	s1		s2		s3		s2		s4a		
Assemblage	55Pn45Py$_b$		60Py$_v$30Pn10Cp		45Cp35Pn20Py$_v$		60Cp25Py$_v$15Pn		40Py$_b$40Pn20Cp		
Analyse #	ab_5	ab_6	ab_7	ab_8	ab_9	ab_10	ab_11	ab_12	ab_13	ab_14	ab_15
Ablated phase(s)	Py (±Pn±Cp)	Pn (±Py)	Py (±Cp)	Pn (±Cp±Py)	Cp	Py (±Cp±Pn)	Py (±Cp)	Cp (±Pn)	Py (±Pn±Cp)	Cp (±Pn)	Pn-Cp
Ni	1642	253964	297	190481	1224	12747	191	6457	1534	7206	356799
Zn	0.75	70.0	0.168	58.0	0.23	4.27	0.122	1.23	1.25	1.33	103
As	6.96	0.520	13.1	0.25	<0.043	0.496	0.490	3.70	5.09	0.141	0.129
Se	102	102	29.8	123	55.1	100	30.6	166	148	132	261
Te	14.0	6.40	<0.057	2.11	0.230	0.308	0.445	1.32	0.354	5.80	4.40
Ag	1.34	2.54	0.576	2.23	0.368	0.453	1.12	17.5	1.62	7.98	21.3
Pb	1.26	2.23	0.278	0.550	0.096	0.950	0.960	3.28	2.88	6.45	32.5
Bi	1.90	0.178	0.07	0.193	<0.0016	0.452	0.182	0.247	0.142	0.107	0.425
S/Se	5,395	3,256	18,139	2,654	6,350	5,375	17,647	2,108	2,973	2,658	1,272
Os	3.91	1.38	269	5.90	<0.0049	74.8	68.1	1.52	8.61	2.90	0.90
Ir	2.37	1.11	384	0.810	0.00	67.1	102	0.547	4.88	1.42	0.23
Ru	5.06	2.92	470	0.880	0.115	136	122	1.61	9.94	2.46	1.61
Rh	6.25	0.01	80.4	0.151	11.8	92.4	2.69	10.04	19.7	12.0	0.443
Pt	1.68	0.201	0.330	0.577	0.0046	1.36	0.0068	0.0026	0.360	1.18	0.399
Pd	1.08	8.97	<0.016	9.04	0.364	1.13	<0.019	0.0660	0.445	1.95	22.85
Au	0.0600	0.0156	0.00140	0.0310	<0.0023	0.0148	0.0103	0.038	0.193	0.174	0.0167

70-222								71335		
s1			s2		s3	s3B	s4	s1	s3	s4
65Pn20Po15Py$_v$			80Pn20Py$_v$		45Py$_b$30Cp25Pn		60Pn40Py$_v$	80Py$_b$20Pn	65Py$_b$35Pn	65Py$_b$35Pn
ab_18	ab_19	ab_20	ab_21	ab_22	ab_23	ab_24	ab_25	ab_28	ab_29	ab_30
Po	60Py40Pn	Pn?	40Py60Pn	Pn	80Py20Pn	95Cp5Py (±Pn)	50Py50Pn	Py	Py	Py
6035	115357	351605	149156	381001	6737	30620	124560	4338	5274	4882
5.32	35.3	112	43.0	128	3.03	8.22	38.6	2.45	2.50	2.08
<0.11	0.87	1.83	4.74	0.85	7.18	6.67	1.69	1.32	3.19	1.32
8.05	167	204	201	160	86.2	99.8	197	19.2	17.8	4.28
4.00	5.85	10.4	28.5	6.46	7.85	7.70	3.79	7.84	7.13	2.90
7.59	3.33	12.8	4.14	2.78	2.34	1068	4.59	2.96	1.76	4.15

5.95	4.07	5.60	2.56	0.390	3.70	6.42	5.92	2.46	1.68	8.59		
1.46	3.65	12.6	2.34	0.179	2.34	1.21	1.43	0.760	1.05	0.31		
49,068	2,459	1,634	2,139	2,181	5,107	3,505	2,231	28,095	30,371	126,188		
20.9	24.2	24.3	21.9	18.2	28.3	4.69	35.0	6.08	8.31	5.76		
14.4	20.9	20.8	19.3	4.85	26.7	2.78	31.8	4.79	1.33	0.970		
16.3	19.7	22.9	20.6	15.4	29.5	3.10	28.1	2.94	1.05	1.38		
1.67	2.04	1.19	0.550	0.412	19.6	15.9	1.91	0.757	1.18	1.28		
3.96	0.910	3.44	14.8	3.55	2.60	1.23	1.46	7.09	10.0	8.82		
3.41	12.3	28.2	20.5	42.7	0.720	5.81	12.4	1.71	1.27	0.700		
5.03	2.28	3.27	1.19	1.34	0.279	4.87	1.39	1.71	1.65	2.35		

All data reported in ppm

b "blocky" pyrite (see text); *v* vermicular pyrite (see text)

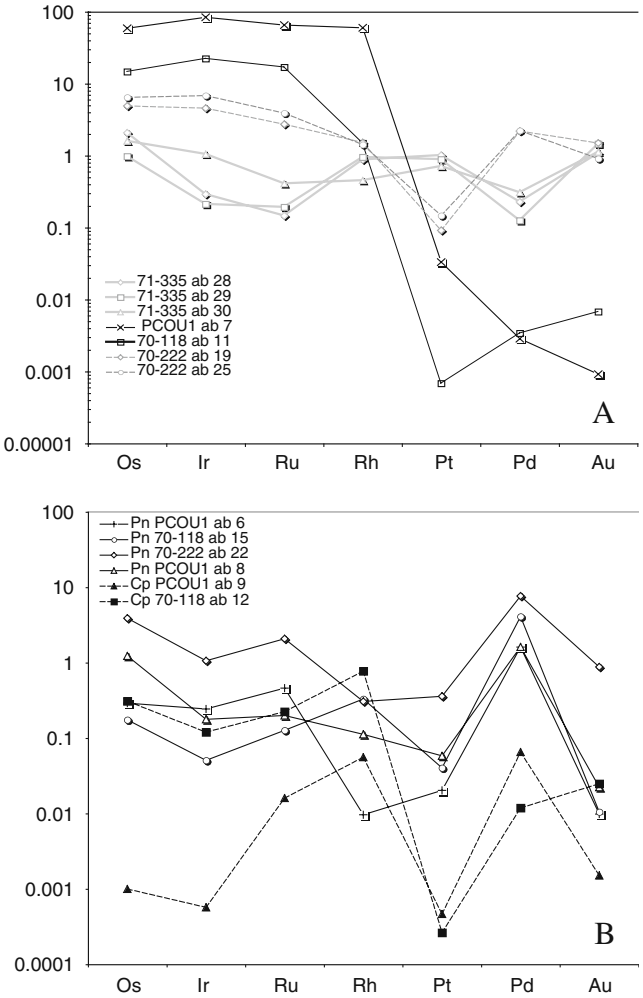

Fig. 5 C1—chondrite normalized PGE patterns of pyrite (**a**), pentlandite and chalcopyrite (**b**) (in-situ laser-ablation ICPMS analyses). Vermicular pentlandite-pyrite intergrowths (PCOU1 ab 7; 70-118 ab 11); coarse-grained pyrite (71-335 ab 28; 71-335 ab 29; 71-335 ab 30); coarse-granular pyrite analyses contaminated by pentlandite (70-222 ab 19; 70-222 ab 25)

ite in poikilitic pyrite blebs and (c) occurrence of vermicular pyrite cutting across the contact between pentlandite and chalcopyrite. Microstructures and shapes of pyrite-rich grains argue for a pre-existing pentlandite-chalcopyrite-(pyrrhotite) assemblage, more metal-rich than the monosulfide solid solution. Pyrite pseudomorphs preserve the denticulated shapes of pentlandite + chalcopyrite blebs which are solidification products of highly wetting, metal-rich, sulfide melts (metal/sulfur atomic ratio >1 in the Cu-Fe-Ni-S system; Bockrath et al. 2004; Lorand et al. 2008, 2010). Because such metal-rich sulfide blebs are locally preserved side-by-side with pyrite-rich grains, we conclude that the pyrite-producing reactions did operate on a very localized scale. If exsolved from mantle-derived sulfides, the pyrite should be homogeneously distributed, at least at the scale of a hand-sample, because the fugacity of sulfur in

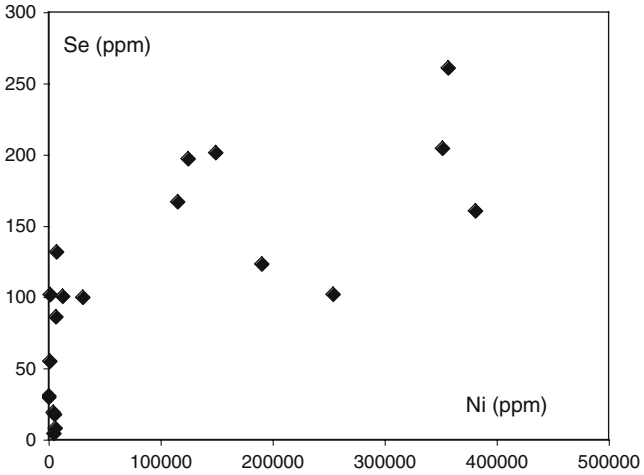

Fig. 6 Selenium vs. nickel diagram for base metal sulfides from pyrite-rich lherzolites (laser-ablation ICPMS in-situ analyses). Nickel and selenium contents measured by LA-ICPMS

mantle peridotites is tightly buffered by the heterogeneous equilibrium olivine-orthopyroxene-monosulfide solid solution (Eggler and Lorand 1993).

The cooling history of metal-rich sulfide melt precursor of pentlandite + chalcopyrite rich assemblages have been discussed in detail in previous studies (Lorand 1989a, b, 2008; 2010). Both sulfides crystallize from subsolidus decompositions and reaction between Mss, Cu-rich solid solution (intermediate solid solution) and high-temperature heazlewoodite. Yet some experimental studies did produce a high-temperature pentlandite polymorph at 850°C (Sugaki and Kitakaze 1998), blocky pentlandite is thought to be stable at lower temperature (<600°C). Cubic intermediate solid solution inverts to tetragonal chalcopyrite at 557°C (Barton 1973). In terms of sulfur fugacity (Fig. 7), experiments on pentlandite-chalcopyrite assemblage define a logfS_2 path below the FMQ-Po fS_2 reference buffer (Kaneda et al. 1986; Peregoedova and Ohnenstetter 2002; Makovicky 2002). This estimate is supported by the occurrence of Pt alloys instead of Pt sulfides in Eastern Pyrenean peridotites (Fig. 7). Note that a metal-rich sulfide melt cooling isochemically cannot produce pyrite as it evolves at too low fS_2 and on the wrong side of the Mss barrier.

By contrast, the assemblage pentlandite + pyrite + chalcopyrite reflects excursion within the logfS_2-T area of pyrite + chalcopyrite stability, i.e. well above the FMQ-Po reference curve. This cooling path can be explained ony by addition of S to host peridotites. The temperature range at which this sulfurization occurred can be estimated only qualitatively because phase relationships within the quaternary system Cu–Fe–Ni–S are not determined with sufficient precision at T<550°C (Fleet 2006). Pyrite is stable at temperature up to 810°C for 0.5 GPa total pressure (Toulmin and Barton 1964). However, as shown by Fig. 4, co-crystallization of pentlandite and pyrite is precluded at T>300°C by the Mss (Misra and Fleet 1973; Craig 1973; Fleet 2006). Thus, to explain symplectite-like pentlandite + pyrite microstructures, one may argue that pentlandite was first sulfurized into Mss at T above 300°C; then, upon cooling below 300°C, the Mss broke down into pentlandite + pyrite symplectites, which nucleated onto relict Pn nuclei (Fig. 3). Pyrite blebs enclosed within the

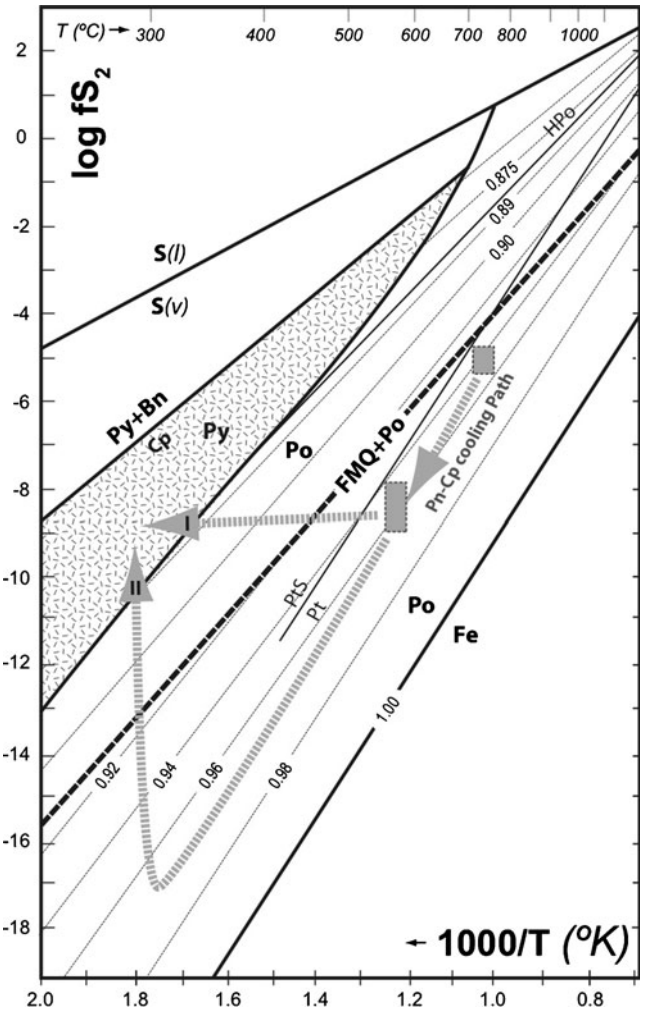

Fig. 7 Log fS_2 versus 1/T (°K) diagram showing two possible sulfurization paths that produced pyrite in Pyrenean peridotites (*dashed arrows*). *Dashed line* (bornite-out; Lusk and Bray 2002) delineates the maximum fS_2 values that were produced by sulfurization reactions in pyrite-rich Pyrenean lherzolites. Pyrrhotite isopleths from Toulmin and Barton (1964) were converted into metal-to-sulfur ratios for clarity. FMQ-Po buffer from Eggler and Lorand (1993). Pyrrhotite-iron (Fe–Po) and sulfur vapor-sulfur liquid (S(v)–S(l)) reaction curves from Toulmin and Barton (1964) and pyrrhotite-pyrite (Po-Py) reaction curve from Lusk and Bray (2002). Platinum-platinum sulfide (Pt-PtS) reaction curve after Barin (1995). The sub-solidus cooling path of the metal-rich sulfide assemblage pentlandite + chalcopyrite prior to pyrite crystallization (squares) is based on log fS_2-T estimates of Kaneda et al. (1986), Peregoedova and Ohnenstetter (2002) and Makovicky (2002)

pentlandite may have started to nucleate at temperature between 600 and 300°C, prior to pentlandite, from the most S-rich Mss compositions that plot toward the S-rich solvus in Fig. 4. As chalcopyrite is devoid of inversion twining, the maximum temperature for crystallization of poikilitic pyrite replacing the chalcopyrite (Fig. 3) is about 550°C, the temperature of inversion of cubic intermediate solid solution to tetragonal chalcopyrite (Barton 1973). Symplectite-like intergrowths between chalcopyrite, pyrite and pentlandite probably exsolved from Cu-rich Mss. Monosulfide solid solution, chalcopyrite and pyrite can coexist below 335°C, but this temperature raises to 420°C for bulk-sulfide compositions containing 10 wt.% Ni (Craig and Kullerud 1969; Lusk and Bray 2002 and references therein).

To summarize, one may assume that pyrite formed between c.a. 300 and 600°C in the smallest Eastern Pyrenean peridotites bodies. Chalcophile element contents and PGE systematics support a different crystallization scheme for symplectite-like pyrite (Mss-Iss decomposition products) and coarse-granular and/or poikilitic pyrite. The former shows Mss-like C1-chondrite normalized PGE patterns, in agreement with their derivation from Mss. The preferential partitioning of IPGEs (Os, Ir, Ru and Rh) into pyrite relative to pentlandite is consistent with their strong preference for octahedral sites, which predominate in pyrite and in its structural analogous laurite (Barkov et al. 1997) and the strong similarity in terms of ionic radii between Fe and Os, Ir and Ru (e.g. Li et al. 1996; Barnes et al. 2001). The same behaviour was observed for Co (Lorand 1989b). The small grain size of eutectoid pyrite counterbalanced the slow diffusion rate of PGE into pyrite ($D<10^{-22}$ $m^2.s^{-1}$at 500°C) as measured for Os by Brenan et al. (2000). Chalcophile elements (e.g. Pd and Zn) were preferentially partitioned into pentlandite, in agreement with their lesser affinity for octahedral sites.

Poikilitic and massive ("blocky") pyrite grains display gradational decrease of PGE contents either because temperature was too low for the IPGE's to diffuse inside pyrite symplectites or, more likely, the pyrite crystallized directly from S-rich fluids, as discussed below.

Country-rock sulfur assimilation

Sulfurization reactions indicate sulfur addition from an external source. Pyrite-rich lherzolites show whole-rock S contents higher by ca. 20–30% compared to pyrite-poor lherzolites of similar fertility (Table 1; Lorand 1989a, 1991). Pyrenean pyrite shows much higher S/Se > compared to mantle-derived sulfides (2.10^3–4.10^3; Guo et al. 1999; Hattori et al. 2002; Lorand et al. 2003). This ratio is quite uniform and independent of pyrite habits, suggesting that it was not altered by exchange of Se between pentlandite and pyrite. Sedimentary rocks show S/Se ratios of 10^5 or more, as obtained for the Eastern Pyrenean pyrite occurrences (Ripley 1990; Ripley et al. 1999). Metasedimentary country rocks are thus potential contaminants for sulfur, due to the abundance of S-rich minerals (pyrite, scapolites, Ca-sulfates; Golberg and Leyreloup 1990). Assimilation of sulfur from reduced lagoonal sediments may also account for the negative $\delta^{34}S$ composition of pyrite (up to−10‰) reported by Chaussidon and Lorand (1990) in some samples from Lherz. It is also consistent with the other evidence of peridotite-country rocks exchanges documented in some pyrite-rich bodies (e.g. low-pressure CO_2 secondary inclusions, enrichment in gold and unradiogenic strontium at Caussou).

Assimilation of sulfur in crustal contamination processes is usually ascribed to migration of elemental sulfur (liquid or vapor) released by the breakdown of pyrrhotite into pyrite, which occurs at 0.5 GPa total pressure (Kullerud and Yoder 1959). Pure liquid or vapor sulfur is so reactive with mafic rocks that it is automatically converted into sulfides by extracting Fe and Ni from olivine and pyroxenes (Naldrett and Gasparini 1971; Libaudé and Sabatier 1980). There is no evidence for such sulfides in Pyrenean peridotites: as discussed above, pyrite is invariably associated with mantle-derived BMS. Further, such sulfur liquid is expected to inherit from their sedimentary source extremely low IPGE abundances and to have an extremely PGE fractionated pattern. This is not compatible with the PGE abundance patterns reported here for Eastern Pyrenean pyrites.

Although some pyrite-rich lherzolite bodies caused contact metamorphism of their surrounding country rocks (e.g. Fontête Rouge; Bestiac; Lacroix 1895), contact metamorphism is not believed to be main source of S contamination because i) its extent is highly variable from one massif to another (Monchoux 1970), ii) small peridotite bodies are expected to release less heat that large, km-sized slices. Significantly, the largest massifs of Prades-Pic de Géral to the east, and Lherz-Freychinède to the west are on average pyrite-poor. Assimilation of sulfur by Eastern Pyrenean peridotites is better explained by the middle Cretaceous Pyrenean metamorphism resulting from extensive lithospheric thinning beneath the North Pyrenean fault. Metamorphic peak conditions documented by Golberg and Leyreloup (1990) involve temperatures close to that inferred for pyrite crystallization (550–650°C, for a maximum pressure of 0.3–0.4 GPa). Regional Pyrenean metamorphism released sulfur-rich hot, alkaline (H_2O)–CO_2–Cl fluids via decarbonation reactions (Dauteuil and Ricou 1989; Golberg and Leyreloup 1990) and heating of Triassic and Liassic metaevaporites (Golberg and Leyreloup 1985; J-L Bodinier, personal communication to J.-P. Lorand). Chlorine-

rich CO_2 fluids also account for the Au-rich pyrite compositions because at these temperatures Au is soluble as chloride complexes in addition to base metals (Cameron and Hattori 1987; Fleet and Wu 1995).

Grain boundary percolation of CO_2-rich fluids in lherzolitic matrix is thought to be very low (Menzies and Dupuy 1991). C–H–O vapors do not form grain boundary films and tend to remain immobile as a result of permeabilities that approach zero because the pore space is not interconnected (Watson and Brenan 1987; Frezzotti et al. 2002). Likewise, there is no obvious relationship between pyrite abundance and degree of plastic deformation of host peridotites. Plastic deformation in peridotite massifs ceased at 700–750°C and $P>0.8$ Gpa, i.e. prior to emplacement into crustal sedimentary rocks (Conquéré and Fabriès 1984; Fabriès et al. 1991). The pyrite-rich samples studied here show coarse-granular to protogranular microstructures (average grain size=0.5–1 cm across) almost devoid of shearing deformation. Thus, it is inferred that most of the sulfur contamination occurred via forcefull injection into structural discontinuities (cracks, veins, fracture planes). As shown by Golberg and Leyreloup (1990), fracturing played an essential role in heat and fluid transfer during Pyrenean regional metamorphism (see also Dauteuil and Ricou 1989). At the scale of a thin-section, decompression-related cracks may have driven sedimentary sulfur inside olivine-hosted pseudo-primary sulfide inclusions, thus generating pentlandite-vermicular intergrowths as represented Fig. 3b. As some of these inclusions are devoid of fracture planes, entrapment of contaminated BMS during fluid-assisted hydrothermal recrystallization of olivine cannot be ruled out. This would account for the abundance peak of olivine-hosted BMS inclusion in the small peridotite outcrops of Bestiac. Another evidence of the part played by structural discontinuities in S transfer is the unusual pyrite modal abundances (e.g. 35% in 71-335) in peridotite samples collected close to contacts of the largest Eastern Pyrenean peridotite massifs with the metamorphosed country rocks. This fracture-driven contamination process was greatly enhanced by CO_2-overpressure and brecciations of country rocks. Variable extent of sulfur assimilation, perhaps coupled with temperature variations, are expected to have created sulfur fugacity gradients, which, superimposed to large variations in the initial chalcopyrite/chalcopyrite + pentlandite ratios of mantle-derived sulfides (0–100; Lorand et al. 2008, 2010) generated the wide spectrum of sulfide microstructures and sulfide mineral assemblages now observed in pyrite-rich Eastern Pyrenean lherzolites. Vermicular holes inside pentlandite, and evidence of secondary polycrystalline pyrrhotite replacing the pyrite suggest that even the largest Eastern Pyrenean peridotite massifs may have interacted with S-bearing fluids, although they are on average pyrite-poor. The amount of assimilated sulfur or temperature, or both, were much too low for pyrite to nucleate and to store that crustal sulfur.

Conclusions

Pyrite habits and textural relationships within BMS blebs provide indisputable evidence for crystallization of pyrite from replacement of pre-existing mantle sulfides. Microstructural features of pyrite and in-situ analyses of chalcophile and siderophile trace elements support a process of assimilation of crustal sulfur from the metamorphosed sedimentary country rocks as responsible for pyrite formation. Pyrite S/Se ratios ($>10^5$) are consistent with a sedimentary source for S. Sulfur has reacted to various extent with pre-existing, mantle-derived, metal-rich sulfide assemblages (pentlandite-chalcopyrite). The wide range of pyrite habits characterized by different platinum-group element systematics, depends on the amount of assimilated sulfur. The absence of pyrite or its alteration products (secondary pyrrhotite) in lherzolitic bodies from Central and Western Pyrenees is consistent with decreasing degrees of Pyrenean regional metamorphism in Mesozoic sediments toward the western end of the Pyrenean belt (Fabriès et al. 1991, 1998).

Pyrite may be used for tracking modification of mantle-derived S budgets of orogenic peridotite during tectonic emplacement of orogenic peridotites into the crust. The scarcity of pyrite and the reproducible whole-rock S contents in the largest orogenic peridotite massifs studied so far (e.g. Lherz; Ivrea-Verbano zone; Beni Bousera; Ronda; Lanzo; Horoman) is evidence against significant assimilation of crustal sulfur.

Acknowledgements Olivier Brugier is gratefully acknowledged for his help with the laser ablation microprobe. Financial support was provided by INSU-CNRS grants. The final version of the manuscript was greatly improved thanks to comments of two anonymous reviewers and editorial advises of Associate Editor Giorgio Garuti.

References

Alard O, Griffin WL, Lorand J-P, Jackson S, O'Reilly SR (2000) Non-chondritic distribution of highly siderophile elements in mantle sulfide. Nature 407:891–894

Barin I (1995) Thermochemical data of pure substances. VCH Weinheim, pp 1885

Barkov AY, Halkoaho TAA, Laajoki KVO, Alapieti TT, Peura R (1997) Ruthenian pyrite and nickeloan malanite from the Imandra Layered Complex, Northwestern Russia. Can Miner 35:887–897

Barnes SJ, Van Achterbergh E, Makovicky E, Li C (2001) Proton microprobe results for the partitioning of platinum-group ele-

ments between monosulfide solid solution and sulphide liquid. S Afr J Geol 104:275–286
Barnes SJ, Cox RA, Zientek ML (2006) Platinum-group element, gold, silver and base metal distribution in compositionally zoned sulfide droplets from the Medvezky Creek Mine, Noril'sk, Russia. Contrib Mineral Petrol 152:187–200
Barton PB (1973) Solid solutions in the Cu–Fe–S system. Part 1. The Cu–S and the Cu–Fe–S joins. Econ Geol 68:445–463
Bockrath C, Ballhaus C, Holzheid A (2004) Fractionation of the platinum-group elements during mantle melting. Science 305:1951–1953
Brenan JM, Cherniak DJ, Rose LA (2000) Diffusion of osmium in pyrrhotite and yrite: implications for closure of the Re–Os isotopic system. Earth Planet Sci Lett 180:399–413
Cameron EI, Hattori K (1987) Archean gold mineralization and oxidized hydrothermal fluids. Econ Geol 82:1177–1191
Chaussidon M, Lorand J-P (1990) Sulphur isotope composition of orogenic spinel lherzolite massifs from Ariège (Northeastern Pyrennes, France): an ion microprobe study. Geochim Cosmochim Acta 54:2835–2846
Conquéré F (1978) Pétrologie des complexes ultramafiques de lherzolite à spinelle de l'Ariège (France). Thesis, Univ Paris VI, pp 333 (unpublished)
Conquéré F, Fabriès J (1984) Chemical disequilibrium and its thermal significance in spinel peridotites from the Lherz and Freychinède ultramafic bodies (Ariège, French Pyrenees). In: Kornprobst J (ed) Proc 3rd Int Kimberlite Conf II The mantle and crust mantle relationships pp 319–334
Craig JR (1973) Pentlandite-pyrrhotite and other low-temperature relations in the Fe–Ni–S systems. Am J Sci 273:496–510
Craig JR, Kullerud G (1969) Phase relations in the Cu–Fe–Ni–S system and their application to magmatic ore deposits. Econ Geol Monogr 4:344–358
Dauteuil O, Ricou LE (1989) Une circulation de fluides de haute température à l'origine du métamorphisme crétacé nord-Pyrénéen. Geodinamica Acta 3:237–250
Dauteuil O, Raymond D, Ricou LE (1987) Brèches de fracturation hydraulique dans la zone métamorphique des Pyrénées, exemples à l'Est du Saint-Barthélémy. C R Acad Sci Paris 304:1025–1028
Downes H, Bodinier J-L, Thirlwall M-F, Lorand J-P, Fabriès J (1991) REE and Sr–Nd isotopic geochemistry of Eastern Pyrenean peridotite massifs: sub-continental lithospheric mantle modified by continental magmatism. In: Menzies MA, Dupuy C, Nicolas A (eds) Orogenic Lherzolites and Mantle Processes J Petrol Special Volume, pp 97–115
Duke JM, Naldrett AJ (1976) Sulfide mineralogy of the Main Irruptive, Sudbury, Ontario. Can Miner 14:450–461
Eckstrand OR (1975) The Dumont serpentinite: a model for control of nickeliferous opaque mineral assemblages by alteration reactions in ultramafic rocks. Econ Geol 70:183–200
Eggler DH, Lorand J-P (1993) Mantle sulfide oxybarometry. Geochim Cosmochim Acta 57:2213–2222
Fabriès J, Bodinier J-L, Dupuy C, Lorand J-P, Benkerrou C (1989) Evidence for modal metasomatism in the orogenic spinel lherzolite body from Caussou (Northeastern Pyrenees, France). J Petrol 30:199–228
Fabriès J, Lorand J-P, Bodinier J-L, Dupuy C (1991) Evolution of the upper mantle beneath the Pyrenees: evidence from orogenic spinel lherzolite massifs. In: Menzies MA, Dupuy C, Nicolas A (eds) Orogenic Lherzolites and Mantle Processes J Petrol Special Volume, pp 55–76
Fabriès J, Lorand J-P, Bodinier J-L (1998) Petrogenesis of some Central and Western Pyrenean peridotite massifs. Tectonophysics 292:145–167
Fleet ME (2006) Phase equilibria at high-temperatures. In: Vaughan DJ (ed) Rev Mineral Geochem vol 61, pp 365–419
Fleet ME, Wu TW (1995) Volatile transport of precious metals at 1,000°C: speciation, fractionation, and effect of base-metal sulfide. Geochim Cosmochim Acta 59:487–495
Frezzotti ML, Andersen T, Neumann E-R, Simonsen SL (2002) Carbonatite melt-CO_2 fluid inclusions in mantle xenoliths from Tenerife, Canary Islands: a story of trapping, immiscibility and fluid-rock interaction in the upper mantle. Lithos 64:77–96
Garuti G, Gorgoni C, Sighinolfi GP (1984) Sulfide mineralogy and chalcophile and siderophile element abundances in the Ivrea-Verbano mantle peridotites (Western Italian Alps). Earth Planet Sci Lett 70:69–78
Golberg JM, Leyreloup AF (1985) Mise en évidence de fluides mantelliques dans la zone nord-Pyrénéenne (région de lherz)-: la formation bréchique du col d'Agnes. C R Acad Sci Paris 300:71–74
Golberg J, Maluski H (1988) Données nouvelles et mise au point sur l'âge du métamorphisme Pyrénéen. C R Acad Sc Paris II 306:429–435
Golberg JM, Leyreloup AF (1990) High temperature-low pressure Cretaceous metamorphism related to crustal thinning (Eastern North Pyrenean Zone, France). Contrib Mineral Petrol 104:194–207
Guo J, Griffin WL, O'Reilly SY (1999) Geochemistry and origin of sulfide minerals in mantle xenoliths: Qilin, Southeastern China. J Petrol 40:1125–1151
Hall AJ (1986) Pyrite-pyrrhotine redox reactions in nature. Miner Mag 50:223–228
Hattori KH, Arai S, Clarke DB (2002) Selenium, tellurium, arsenic and antimony contents of primary mantle sulfides. Can Miner 40:637–650
Kaneda H, Takenouchi S, Shoji T (1986) Stability of pentlandite in the Fe–Ni–Co–S system. Miner Deposita 21:169–181
Klein F, Bach W (2009) Fe–Ni–Co–O–S phase relations in peridotite-seawater interactions. J Petrol 50:37–59
Kogiso T, Suzuki T, Shinotsuka K, Uesugi K, Takeuchi A, Suzuki Y (2008) Detecting micrometer-scale platinum-group minerals in mantle peridotite with microbeam synchrotron radiation X-ray fluorescence analysis. Geochem Geophys Geosyst 9:Q03018. doi:10.1029/2007GC001888
Kullerud G, Yoder HS (1959) Pyrite stability in the Fe–S system. Econ Geol 54:534–569
Lacroix A (1895) Les phénomènes de contact de la lherzolite et de quelques ophites des Pyrénées. Bulletin de la Carte Géologique de France 6(42):307–446
Lagabrielle Y, Bodinier JL (2008) Submarine reworking of exhumed subcontinentalmantle rocks: field evidence from the Lherz peridotites, French Pyrenees. Terra Nova 20(1):11–21
Li C, Barnes S-J, Makovicky E, Rose-Hansen J, Makovicky M (1996) Partitioning of nickel, copper, iridium, platinum, and palladium between monosulfide solid solution and sulfide liquid: effects of composition and temperature. Geochim Cosmochim Acta 60:1231–1238
Libaudé J, Sabatier G (1980) Contribution à l'étude de la sulfuration des olivines nickelifères en phase vapeur. Mémoire du Bureau des Recherches Géologiques et Minières 97:252–253
Lorand J-P (1985) The behaviour of the upper mantle sulfide component during the incipient serpentinization of "alpine"-type peridotites as exemplified by the Beni Bousera (Northern Morocco) and Ronda (Southern Spain) ultramafic bodies. Tscherm Miner Petr ogr Mitt 34:183–211
Lorand J-P (1989a) Abundance and distribution of Cu–Fe–Ni sulfides, sulfur, copper and platinum-group elements in orogenic-type spinel peridotites of Ariège (Northeastern Pyrenees, France). Earth Planet Sci Lett 93:50–64
Lorand J-P (1989b) Mineralogy and chemistry of Cu–Fe–Ni sulfides in mantle-derived spinel peridotite bodies from Ariège (Northeastern Pyrenees, France). Contrib Mineral Petrol 103:335–349

Lorand J-P (1991) Sulfide petrology and sulfur geochemistry of orogenic lherzolites: a comparative study between Pyrenean bodies (France) and the Lanzo massif (Italy). In: Menzies MA, Dupuy C, Nicolas A (eds) Orogenic Lherzolites and Mantle Processes J Petrol Special Volume, pp 77–95

Lorand J-P, Conquéré F (1983) Contribution à l'étude des sulfures dans les enclaves de lherzolites à spinelle des basaltes alcalins (Massif Central et du Languedoc, France). Bull Minéral 106:585–606

Lorand J-P, Alard O (2001) Geochemistry of platinum-group elements in the sub-continental lithospheric mantle; in-situ and whole-rock analyses of some spinel peridotite xenoliths, Massif Central, France. Geochim Cosmochim Acta 65:2789–2806

Lorand J-P, Pattou L, Gros M (1999) Fractionation of platinum-group elements and gold in the upper mantle: a detailed study in Pyrenean orogenic lherzolites. J Petrol 40:957–981

Lorand J-P, Alard O, Luguet A, Keays RR (2003) Sulfur and selenium systematics of the subcontinental lithospheric mantle: Inferences from the Massif Central xenolith suite (France). Geochim Cosmochim Acta 67:4137–4151

Lorand J-P, Luguet A, Alard O, Bézos A, Meisel T (2008) Abundance and distribution of platinum-group elements in FON-B 93, a matrix-matched orogenic lherzolite (Ariège, French Pyrénées). Chem Geol 248:74–194

Lorand J-P, Alard O, Luguet A (2010) Platinum-group element micronuggetts and refertilization process in the Lherz peridotite. Earth Planet Sci Lett 289:298–310

Luguet A, Lorand J-P, Alard O, Cottin J-Y (2004) A multi-technique study of platinum-group elements systematic in some Ligurian ophiolitic peridotites, Italy. Chem Geol 208:175–194

Lusk J, Bray D (2002) Phase relations and the electrochemical determination of sulfur fugacity for selected reactions in the Cu–Fe–S and Fe–S systems at 1 bar and temperatures between 185 and 460°C. Chem Geol 192:227–248

Makovicky E (2002) Ternary and quaternary phase systems with PGE. In: Cabri LJ (ed) The Geology, Geochemistry, Mineralogy and Mineral Beneficiation of Platinum-Group Elements. Can Instit Min Metall Petrol, Montreal, pp 131–178

Menzies M, Dupuy C (1991) Orogenic massifs; protoliths, process and provenance. In: Menzies MA, Dupuy C, Nicolas A (eds) Orogenic Lherzolites and Mantle Processes J Petrol Special Volume, pp 1–16

Misra K, Fleet ME (1973) The chemical composition of synthetic and natural pentlandite assemblages. Econ Geol 68:518–539

Monchoux P (1970) Les lherzolites Pyrénéennes. Contribution à l'étude de leur minéralogie, de leur genèse et de leurs transformations. Thesis Univ Toulouse, p 180 (unpublished)

Montigny R, Azambre B, Rossy M, Thuizat R (1986) K–Ar study of Cretaceous magmatism and metamorphism in the Pyrénées-: age and length of rotation of the Iberian peninsula. Tectonophysics 129:257–273

Naldrett AJ, Gasparini EL (1971) Archean nickel sulfide deposits in Canada: their classification, geological setting and genesis; with some suggestion as to exploration. Geol Soc Austral, Spec Publ 3:201–226

Naldrett AJ, Craig JR, Kullerud G (1967) The central portion of the Fe–Ni–S system and its bearing on pentlandite exsolution in iron–nickel sulfides ores. Econ Geol 62:826–847

Peregoedova A, Ohnenstetter M (2002) Collectors of Pd, Rh and Pt in a S-poor Fe–Ni–Cu sulfide system at 760°C: experimental data and application to ore deposits. Can Miner 40:527–561

Ravier J, Thiébaut J (1982) Sur l'origine lagunaire des marbres et cronéennes mésozoïques du col d'Agnes (Ariège). CR Acad Sci Paris 294:127–130

Ripley EM (1990) Se/S ratios in the Virginia Formation and Cu–Ni sulfide mineralization in the Babbitt deposit, Duluth Complex, Minnesota. Econ Geol 8:830–841

Ripley EM, Par YR, Li C, Naldrett AJ (1999) Sulfur and oxygen isotopic evidence of country rock contamination in the Voisey's Bay Ni–Cu–Co deposit, Labrador, Canada. Lithos 47:53–68

Sugaki A, Kitakaze A (1998) High-tempertature form of pentlandite and its thermal stability. Amer Miner 83:133–140

Toulmin P, Barton PB (1964) A thermodynamic study of pyrite and pyrrhotite. Geochim Cosmochim Acta 68:641–667

Van Achterbergh E, Ryan CG, Griffin WL (2001) Data reduction software for LA-ICP-MS. In: Sylvester P (ed) Laser-ablation-ICPMS in the earth sciences: principles and applications. St John's, Newfoundland, USA: Min Assoc Canada, Short Course Series 29: 239–243

Vielzeuf D, Kornprobst J (1984) Crustal splitting and the emplacement of Pyrenean lherzolites and granulites. Earth Planet Sci Lett 67:87–96

Watson EB, Brenan JM (1987) Fluids in the lithosphere, 1. Experimentally-determined wetting characteristics of CO_2–H_2O fluids and their implications for fluid transport, host-rock physical properties and fluid inclusion formation. Earth Planet Sci Lett 85:497–515